Article

Considering the Size Distribution of Elements in Particle Matter and Oxidation Potential: Association before and after Respiratory Exposure

Xing Li, Tingting Xu and Ying Guo *

Guangdong Key Laboratory of Environmental Pollution and Health, School of Environment, Jinan University, Guangzhou 510632, China
* Correspondence: yingguo2004@163.com or yingguo2004@jnu.edu.cn

Abstract: Oxidation potential (OP), reflecting the redox activities of particle matter (PM), is considered an optimal measure to explain the biological effects of PM exposure. However, the size resolution of the relationship between OP and chemical composition in PM, especially how the relationship changes after respiratory exposure, has not been well investigated. In this study, size-resolved indoor PM_{10} samples were collected from a waste recycling plant from November to December 2021 using an Anderson eight-stage cascade impactor. OP, measured by a dithiothreitol (DTT) assay (defined as OP^{DTT}), and elements, determined by inductively coupled plasma–mass spectrometry (ICP-MS) in size-resolved PM, were determined to check their relationships and the related human exposure risk. The results indicated that compared with $PM_{0.4}$ and $PM_{0.4-2.1}$, $PM_{2.1-10}$ contributed the most to total OP^{DTT} and its bound elements contributed the most to potential health risks, both before and after respiratory exposure. The association between OP^{DTT} and the elements varied with PM size. Pearson correlation analysis showed that the $PM_{0.4}$- and $PM_{0.4-2.1}$-bound elements were moderate-to-strongly positively correlated with OP_v^{DTT} (r: 0.60–0.90). No significant correlation or dose–response relationship was found in $PM_{2.1-10}$. After respiratory exposure, several $PM_{0.4}$- and $PM_{0.4-2.1}$-bound elements had a moderate-to-strongly positive correlation with deposition fluxes of OP (defined as OP^{Flux}) (0.69–0.90). A generalized linear model analysis showed that the interquartile range (IQR) increase in the PM-bound elements (ng h^{-1}) was associated with a 41.7–58.1% increase in OP^{Flux}. Our study is a special case that enriches the knowledge of the association between OP^{DTT} and the chemical composition of PM of different sizes, especially after respiratory exposure, but the generalizability of the findings to other settings or types of PM may be limited. The associations among OP^{DTT}, other chemical compositions of PM, and human exposure risk merit further research.

Keywords: air particle; oxidation potential; elements; size distribution; respiratory exposure

1. Introduction

Air pollution is one of the most pressing global environmental problems. A growing body of evidence shows that air pollution has significant risks to life and health quality across the world [1,2]. Among the various pollutants in the air, particle matter (PM) contributes the most to adverse health effects, especially for the respiratory and cardiovascular systems [3–5]. In 2019, global ambient $PM_{2.5}$-related deaths and disability-adjusted life years (DALYs) were 4,140,970 and 118.2 million [6]. Of the 13 level-three causes, ischemic heart disease, stroke, pulmonary disease, diabetes mellitus, and lung cancer were the top five contributors to the increase in global deaths and DALYs attributable to ambient $PM_{2.5}$ [6]. Oxidative stress derived from the PM-mediated generation of reactive oxygen species (ROS) in vivo is one of the most important mechanisms that causes damage to the body [7,8].

Depending on specific sources and components, the toxicity of PM varies widely [9,10], which mean that mitigation strategies to reduce PM concentration may not effectively

reduce the effects of exposure to PM pollution on human health. Oxidation potential (OP) is used to monitor the biological effects of PM exposure. Due to being faster and less resource-intensive than cellular assays, acellular assays for OP have led to a rapid increase in OP measurements worldwide. Common acellular OP assays include electron spin (or paramagnetic) resonance, the dithiothreitol assay, the ascorbic acid assay, and the glutathione assay [11]. Previous studies have measured PM OP by using ultrapure water as an extracting solution [12,13]. However, recent toxicological research has broadly assumed that the use of ultrapure water as an extracting solution cannot reflect the physiological conditions in the lungs. For this reason, there is a growing number of studies choosing simulated lung fluids (SLFs) as an extracting solution, and it has been found that the composition and PH of SLFs can affect PM OP. OP assay conditions need to be further investigated [14,15]. Epidemiologic studies have found the relevance of OP measured by acellular assays to health, and OP is more strongly associated with acute cardiac and respiratory endpoints than PM concentration [16,17]. Moreover, OP has been reported to be a potential environmental stressor for chronic diseases [18]. Furthermore, mitigation strategies to reduce PM concentration may not effectively reduce OP [19]. OP has been considered a better measurement than PM concentration to explain the biological effects of PM exposure because OP comprehensively reflects multiple aspects of PM, including chemical compositions, synergistic interactions between chemical species and emission source impacts, redox cycling by complex organics, and oxidative stress delivered by surfaces [11].

Increasing research on the OP of PM and its relationship with chemical composition (e.g., transition metals, water-soluble organic aerosol, etc.) in different countries has reported that transition metals and quinines (PAH derivatives) in PM are the main contributors to OP [13,19,20]. Transition metals (e.g., vanadium (V), chromium (Cr), iron (Fe), nickel (Ni), copper (Cu), manganese (Mn), lead (Pb), zinc (Zn), and cadmium (Cd)), have attracted great attention, as they can catalyze the formation of ROS in the atmosphere [21–23]. In addition, they can consume antioxidants or induce the production of ROS in vivo and result in oxidative stress [7]. PM research on OP and transition metals indicates that relationships vary with particle size and sample collecting areas. For example, significantly positive correlations between OP and heavy metals were found in PM collected from office buildings in Hungary [12], urban outdoor areas in the southeastern USA [13], diesel exhaust [24], and the roadside in the Netherlands [25], while negative or no correlations were reported for PM collected from an urban area of Milan, Northern Italy [26], or central Atlanta, USA [27]. Charrier et al. estimated that 80% of OP in water-soluble PM was due to transition metals (especially Cu and Mn) [28], and Wexler et al. also found that soluble Cu and Mn contributed to 50% and 20% of OP in PM_1 [29].

Although PM compositions show great effects on OP, there is growing interest in the relationship between PM size and ROS activity, because PM size is related to PM deposition efficiency in the respiratory tract. In general, previous research has showed that mass-normalized OP decreased with increasing particle size [25,30]. Volume-normalized OP showed consistent peaks near 2.5 μm across studies [31]. For example, in Atlanta, GA, water-soluble volume-normalized ambient OP peaked within 1–2.5 μm [32]. Similarly, volume-normalized ambient OP in Los Angeles peaked in the 0.18–2.5 μm range [32]. Human respiratory deposition models have been used to calculate the PM deposition efficiency in the respiratory system. Previous research showed that smaller PM (i.e., ultrafine fractions) had a much higher deposition efficiency in the lower parts of the respiratory tract (i.e., pulmonary/tracheobronchial regions) than larger PM, and the respiratory systems functions as an aerodynamic classification system of PM [30,33]. In addition, smaller PM had a higher penetration in the lower parts of the respiratory tract [34]. So, studying the size distribution of OP in PM is of great significance for studying the effects of respiratory exposure to PM pollution on human health. Furthermore, the relationship between PM and metals in PM may change after respiration. Yan et al. observed the OP of PM in the pulmonary region was mainly associated with transition metals, and quinones played only

a minor role [30], while the opposite result was reported by Fang et al. [33]. Although research on the relationship between OP and metals was discussed in previous studies, with attention mostly on $PM_{2.5}$, few studies have considered the size resolution of the relationships between OP and elements in PM, or changes after respiratory exposure.

To solve the above problem, in the present study, atmospheric size-resolved PM was collected by an Anderson eight-stage cascade impactor in a waste recycling plant, where high pollutant levels would benefit the investigation of interrelationships. We measured the concentrations of 21 elements and OP (defined as OP^{DTT}) in PM and discussed the size distribution of OP^{DTT} and elements, and their relationships before and after using respiratory exposure models. Moreover, we estimated the average daily exposure dose (considering deposition fluxes in the respiratory tract) of several elements to workers and the related potential non-cancer and cancer risks. This study is helpful to understand the contribution of heavy metals to OP in PM with different sizes and the related health risks from exposure, and is helpful to predict the chemical compositions in PM based on OP, and further improve the efficiency of monitoring the effects of exposure to PM pollution on human health (by using the OP of PM as a potential indicator).

2. Materials and Methods

2.1. Sampling Information

The sampling site was selected as an indoor waste recycling plant (113.46° E, 23.03° N) in the Panyu district of Guangzhou, South China (Figure S1). Within 5 km of the plant area, there are main roads, material and mold processing companies, automotive parts manufacturing companies, food companies, and many other industrial parks. A lot of metal, plastic, and other wastes from local cities are brought in by trucks, concentrated in the internal area of the plant, then sorted and transported by workers and forklifts to specific working areas. The PM sampling activity was conducted from November to December 2021. The meteorological conditions were stable during the sampling period. Four sites were selected and evenly distributed in the plant area. An Anderson eight-stage cascade impactor (TISCH-Model, TE-20-800, Tisch Environmental Inc., Cleves, OH, USA) equipped with pre-combusted 81 mm diameter quartz fiber filters (Whatman, MA, USA) was used for PM collection. The flow rate of the sampler was set at an average of 28.3 L min^{-1} and PM_{10} sizes were cut at 0.43, 0.65, 1.1, 2.1, 3.3, 4.7, 5.8, and 9.0 μm, respectively, to simulate the human respiratory deposition efficiency of PM_{10}. Three parallel samples were collected at each site and each sample was collected for three days from 7:30 a.m. to 20:00 p.m. A total of 12 samples were collected and used for chemical and statistical analysis.

2.2. Sample Preparation and Instrumental Analysis

Microwave digestion was applied for the pretreatment of filtered mineral and metallic species, which comprises digestion in a microwave oven with an oxidant mixture. A quarter of each filter was cut into pieces, placed in a PTFE digestion vessel with a mixture of 65% HNO_3 (6 mL), 30% H_2O_2 (2 mL), and 40% HF (0.6 mL) [35,36], and digested in a microwave digestion instrument (Mars6 Xpress, CEM, Matthews, NC, USA). Concentrations of 21 elements, including aluminum (Al), potassium (K), calcium (Ca), V, Cr, Mn, Fe, cobalt (Co), Ni, Cu, Zn, arsenic (As), selenium (Se), silver (Ag), cadmium (Cd), tin (Sn), antimony (Sb), barium (Ba), Tl (thallium), mercury (Hg), and Pb, in the digests were determined using inductively coupled plasma–mass spectrometry (ICP-MS, NexION350, PerkinElmer Inc., Waltham, MA, USA).

The OP of the PM samples was measured by the cell-free dithiothreitol (DTT) referred to in a previous study [33]. Redox-active substances can oxidize DTT to its corresponding disulfide (2-nitro-5-thiobenzoic acid) and the DTT consumption rate (OP) is linearly proportional to the redox activity of PM. In general, a quarter filter was ultrasonically extracted with 6.5 mL deionized water (18.2 MΩ cm) for 30 min, and then the extraction was filtered using a syringe equipped with a 0.45 μm pore size PTFE filter. After that, 1.0 mL of the aerosol extract, 3.5 mL potassium phosphate buffer (0.5 mM, pH = 7.4), and

0.5 mL DTT solution (0.5 mM) were incubated at 37 °C in a thermostat water bath. At each time point (5, 10, 15, 20, 25, and 40 min) after the reaction started, 0.1 mL of the reaction mixture was removed and reacted with 0.1 mL of 5 mM dithiobisnitrobenzoic acid solution in phosphate buffer. The reaction product 2-nitro-5-thiobenzoic acid was quantified using a microplate reader at 412 nm. The details of sample preparation are shown in the Supporting Information (SI).

2.3. Quality Assurance, Quality Control, and Data Analysis

Before PM sampling, all filters were burned at 450 °C for 4 h to remove the organic matter. The filters were stored in a dryer for 48 h at a constant temperature (25 °C) and humidity (50%), then weighed before and after sampling and stored in a refrigerator at −80 °C before further treatment. For each sample batch, two samples of urban air particulate matter reference material (5 mg, SRM 1648a, NIST, Gaithersburg, MD, USA), two field blanks, and two solvent blanks were also digested at the same time. The ICP-MS was optimized daily, and the calibration was carried out using the internal standard (^{45}Sc, ^{73}Ge, ^{115}In, and ^{209}Bi at 50 μg L in 1% HNO_3) during element analysis. The correlation coefficient of the standard curve was 0.9999. Each sample was measured three times by the instrument, and the relative standard deviations (RSDs) needed to be less than 3%; otherwise, the sample was re-measured. The recoveries of elements in the urban air particulate matter SRM were within the allowable ranges of the certified values ($100 \pm 20\%$). Elements of blank quartz filters were well below those of the samples measured and were subtracted from the loaded filters in the above analysis. The limit of detection (LOD) was defined as corresponding to three times the standard deviation of the solvent blank. The results of the quality assurance and quality control are shown in Table S1.

Two field blanks and two duplicate samples were included in each experiment to ensure the reproducibility of PM OP^{DTT}. The DTT consumption rates of the blank quartz filters were well below those of the samples measured and were subtracted from the samples measured. The relative standard deviations (RSDs) of two duplicate samples were less than 5%.

SPSS software version 25 was used for the statistical analysis. Kolmogorov–Smirnov was used to examine the normality of the data. Pearson correlation and univariate linear regression analysis were conducted to explore the association between OP^{DTT} and the selected elements in the PM before and after respiratory exposure. A generalized linear model was used to estimate the relationship between OP^{DTT} and the quartiles of the selected elements in the PM before and after respiratory exposure. Statistical significance was set at $p < 0.05$.

2.4. Human PM Exposure via Respiratory and Health Risk Assessment

The simplified human respiratory deposition model created by the International Commission on Radiological Protection (ICRP) was used to calculate the PM deposition efficiency in the respiratory systems of factory workers. The advantages of the ICRP model mainly involve its wide applicability to the cohort population, including occupational workers, as well as full consideration of human respiratory exchange ratios under diverse environmental conditions (e.g., working or daily life) and the properties (e.g., hygroscopicity and solubility) of the particles and retention mechanisms in respiratory tracts based on the fact that not all size-fractioned particles can be absorbed effectively [37,38]. The deposition efficiency (DE) of particles with a specific size range in the head airway (HA), tracheobronchial (TB), and pulmonary alveoli (PA) regions (referring to DF$_{HA}$, DF$_{TB}$, and DF$_{AR}$, respectively) is calculated by

$$DE_{HA} = IF \times \left[\frac{1}{1 + \exp(6.84 + 1.183\ln Dp)} + \frac{1}{1 + \exp(0.924 - 1.885\ln Dp)} \right], \; IF = 1 - 0.5 \times \left(1 - \frac{1}{1 + 0.00076Dp^{2.8}} \right),$$

$$\text{DE}_{\text{TB}} = \frac{0.00352}{\text{Dp}} \times \left[\exp\left(-0.234(\ln\text{Dp} + 3.40)^2\right) + 63.9\exp\left(-0.819(\ln\text{Dp} - 1.61)^2\right) \right],$$

$$\text{DE}_{\text{PA}} = \frac{0.0155}{\text{Dp}} \times \left[\exp\left(-0.416(\ln\text{Dp} + 2.84)^2\right) + 19.11\exp\left(-0.482(\ln\text{Dp} - 1.362)^2\right) \right],$$

where IF is the inhalation factor of particles in different stages and Dp is the geometric mean particle size (μm).

The deposition fluxes (DF) of OP (defined as OP^{Flux}) and the elements were estimated based on PM deposition efficiency as follows:

$$\text{DF} = \sum (\text{DE} \times C) \times \text{R}_{\text{inh}},$$

where C is $\text{OP}_{\text{v}}{}^{\text{DTT}}$ (air volume-normalized OP^{DTT}) and the concentration of elements in the PM; and R_{inh} is the human inhalation rate ($\text{m}^3 \text{ h}^{-1}$). Here, the inhalation rate was assumed to be 0.66 $\text{m}^3 \text{ h}^{-1}$, according to the workers' age ranges (30–50 years) [39].

The health risks from exposure to PM-bound heavy metals and metalloids (e.g., V, Cr, Mn, Fe, Co, Cu, Zn, As, Cd, Pb, and Tl) were investigated using models developed by the US Environmental Protection Agency [40]. Also, we considered the inhalation exposure process based on deposition fluxes. The average daily intake of an element, and related potential non-cancer risk hazard quotient (HQ) and cancer risk, respectively, caused by non-carcinogens and carcinogens, were evaluated as follows:

$$\text{DI} = \frac{\text{DF} \times \text{ET} \times \text{EF} \times \text{ED}}{\text{BW} \times \text{AT}} \times \text{CF},$$

$$\text{HQ} = \frac{\text{DI}}{\text{RfD}},$$

$$\text{Cancer risk} = \text{DI} \times \text{SF},$$

where DI is the daily intake ($\text{mg kg}^{-1} \text{ day}^{-1}$), RfD is the reference dose ($\text{mg kg}^{-1} \text{ day}^{-1}$), and SF is the cancer slope factor (kg day mg^{-1}). Other definitions, units, and recommended values used in the equations are listed in Table S2. The RfD and SF of each element are listed in Table S3. In this study, the concentrations of Cr (VI) were estimated based on a concentration ratio of Cr (VI) to total Cr of 0.13 [41]. HQ > 1 suggests the existence of significant non-carcinogenic health risk of an element, while HQ ≤ 1 indicates the non-carcinogenic risk of the element can be accepted or ignored [42]. As for carcinogenic risk, the potential risk is serious when the cancer risk is >10^{-4}, can be ignored when the cancer risk is ≤10^{-6}, and can be accepted when the cancer risk is between 10^{-6} and 10^{-4} [43].

3. Results and Discussion

3.1. Size Distribution of Elements and OP^{DTT} in PM

Elements: The average concentration of PM_{10} at all sites ranged from 115 to 435 μg m^{-3}. The average total concentration of PM_{10}-bound elements during the study period was 32.2 ± 10.7 μg m^{-3}, accounting for 14.9 ± 8.39% of PM_{10} mass (Table S4). Concentrations of most elements in the PM of the plant were higher than those in the outdoor air of Guangzhou [44], indicating the plant is a potential pollution source affecting the surrounding environment.

For individuals, levels of V, Fe, and Cu had a significant unimodal peak at 9.0–10 μm (Figure S2), with more than 70% of mass enriched in $\text{PM}_{2.1-10}$. Concentrations of Cd and Tl had bimodal peaks with one major peak at 9.0–10 μm and one minor peak at 0.43–2.1 μm, with more than 60% of mass enriched in $\text{PM}_{2.1}$. For others, concentrations of Cr, Mn, Pb, and Ba had bimodal peaks with one major peak at 9.0–10 μm and one minor peak at 4.7–5.8 μm. Moreover, V, Cu, and Fe had an almost even distribution at 0–3.3 μm. The size distribution of PM-bound elements in our waste recycling plant was different from other research in the urban areas of Beijing and Tianjin, China [45,46], where most elements were bimodal with peaks at 0.43–1.1 and 4.7–5.8 μm, respectively. Also, the contributions of $\text{PM}_{2.1-10}$-bound elements to total elements in the two studies were lower than the value

in our study, because As, Pb, and other trace elements were more easily enriched in $PM_{2.1}$ in their studies [45,46]. The size distribution of PM-bound elements in our study was also different from outdoor research in Cochin, India, where Cu and Pb were characterized by unimodal size distribution with a peak at 0–2.1 µm [47].

Enrichment Factor (EF) is usually used to study the enrichment degree of inorganic elements in multiple environmental media (e.g., air PM and road dust) and to distinguish whether it arises from a natural source or anthropogenic source [48,49]. In this study, we selected Al as the reference element, because Al is stable, immune to human interference, and is widespread in the Earth's crust. The reference crustal element concentrations of Guangdong province in China were selected as the background value [47,49,50]. The details of the EF calculation method are shown in the Supporting Information (SI). When the EF is less than 1, it indicates the inorganic elements are barely enriched and natural sources (e.g., rock and soil) are the important sources, while a value higher than 10 indicates that inorganic elements are moderately to very enriched, and anthropogenic emissions are the main source (Table S5). The estimated results indicated that the elements in the PM of the plant with different sizes had different enrichment degrees and sources (Table S6). For example, Ca had slight enrichment ($1 \leq EF < 10$) in $PM_{0.4}$ and was affected by a mix of natural and anthropic sources, but had almost no enrichment in $PM_{0.4–2.1}$ or $PM_{2.1–10}$ and was affected by natural sources ($EF < 1$). Cu, Ba, and Pb in $PM_{0.4–2.1}$ and $PM_{2.1–10}$ with moderate enrichment ($10 \leq EF < 100$) were mainly affected by anthropic sources. Similarly, Zn, As, Cd, and Sn in PM_{10} with high enrichment ($100 \leq EF < 1000$) were mainly affected by anthropic sources. Therefore, the elements in the plant were mainly affected by anthropic activities.

OP^{DTT}: OP_m^{DTT} is the mass-normalized ROS activity indicating the intrinsic potency and aerosol toxicity of PM driven by a mix of redox-active PM constituents, and OP_v^{DTT} is the air volume-normalized ROS activity indicating the redox activity directly proportional to sample air volume [51]. The average OP_v^{DTT} and OP_m^{DTT} values of PM_{10} at the different sites were 2.35–3.16 nmol min^{-1} m^{-3} and 8.41–18.6 pmol min^{-1} $µg^{-1}$, respectively (Table S4). We summarized the results reported in the research on the OP of PM around the world (Table S7) and found that OP values were affected by several factors, including but not limited to, weather conditions, PM aging degree, and PM compositions.

OP_m^{DTT} had three peaks with one major peak at 0.43–0.65 µm and two minor peaks at 4.7–5.8 µm and 9–10 µm (Figure 1), which was similar to the PM collected from the roadside and outdoor urban areas of Atlanta, Georgia, USA [33], but different from the PM collected on haze and no-haze days in Shanghai, China, where OP_m^{DTT} had a unimodal peak at 0.32–0.56 µm [30].
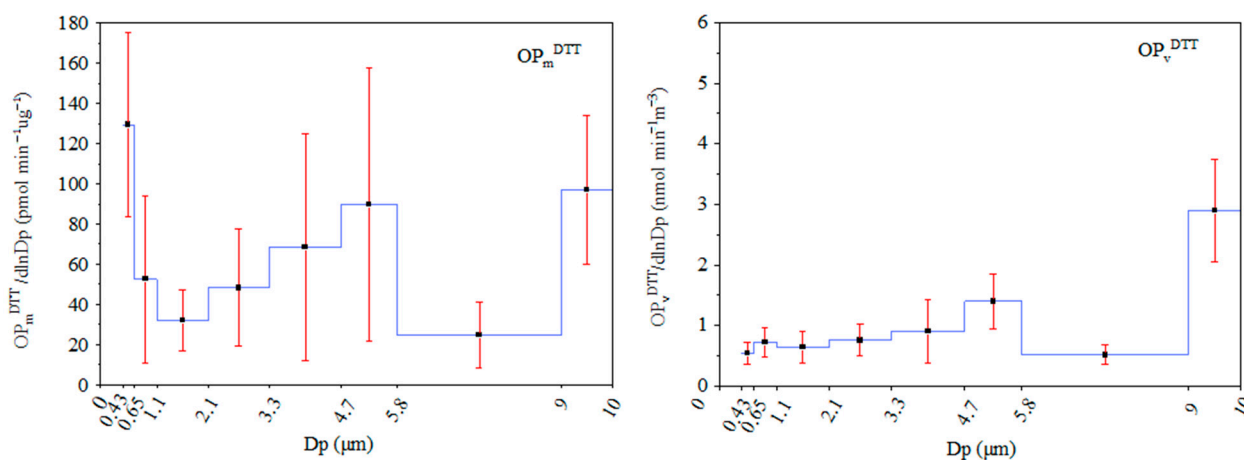

Figure 1. The size distribution of mean OP_m^{DTT} (pmol min^{-1} $µg^{-1}$) and OP_v^{DTT} (nmol min^{-1} m^{-3}) of PM in the waste recycle plant, South China. (Error bars in red refer to the standard deviations ($n = 12$); Dp is the particle diameter (µm)).

For OP_v^{DTT}, the dimensional distribution indicated there was one major peak for 9–10 μm, and two minor peaks for 4.7–5.8 μm and 0.65–1.1 μm, respectively (Figure 1). The distribution pattern of OP_v^{DTT} in the PM we collected from the waste recycling plant was different from the PM from the roadside and indoor and outdoor urban homes, where OP_v^{DTT} usually had a unimodal peak in $PM_{2.5}$ [30,33]. It should be noted that the size distribution of OP_v^{DTT} was similar for several elements, such as V, Mn, Pb, and Ba, indicating the OP_v^{DTT} of PM might be affected by these elements. Furthermore, $PM_{2.1-10}$ contributed the most (46–51%) to the total OP_v^{DTT} due to having the largest mass in our study, while ultrafine/fine PM was reported to have a major contribution to OP in previous other studies [30,33,52]. Our results indicate the oxidative capacity of $PM_{2.1-10}$ should be considered in some special environments.

3.2. Respiratory Deposition of Elements and OP^{DTT} of PM

Elements: The deposition efficiency of all size-resolved PM in the HA, TB, and PA regions was calculated by the ICRP models (Figure S3); then, the efficiency was used to estimate the deposition flux of several selected PM-bound elements (according to the toxicity and content in the PM) in those areas of the respiratory tract based on a hypothetical inhalation rate of 0.66 m^3 h^{-1}. The total deposition flux of the selected elements (V, Cr, Mn, Fe, Co, Cu, Zn, As, Cd, Pb, and Tl) was up to $5.95 \times 10^3 \pm 1.32 \times 10^3$ ng h^{-1} in the whole respiratory tract (Table S8). The average deposition fluxes (efficiencies) of the selected elements were 0.07–4890 ng h^{-1} (47–79%), 0.00–171 ng h^{-1} (~3%), and 0.01–262 ng h^{-1} (4–9%) in the HA, TB, and PA regions of the respiratory tracts, respectively (Table S8 and Figure 2). Additionally, $PM_{2.1-10}$ contributed the most to element deposition in the whole human respiratory tract (average > 80%), especially for V, Cr, Mn, Fe, Co, Cu, Zn, As, and Pb.
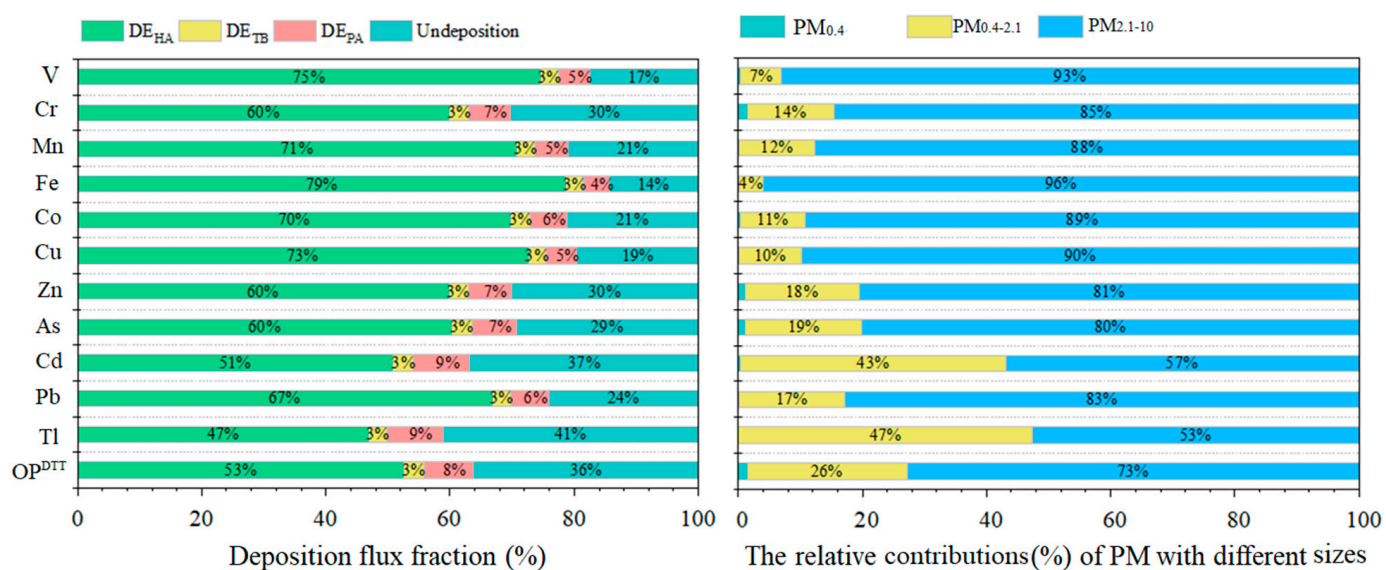
Figure 2. Deposition flux fractions of elements and OP^{DTT} of PM_{10} and the relative contributions of PM with different sizes to total elements and OP^{DTT} of PM_{10} in the whole respiratory tract. Note: head airway, HA; tracheobronchial, TB; and pulmonary, PA. Un-deposition is elements and OP^{DTT} of PM_{10} not deposited in respiratory tract during respiration. The average deposition flux of elements and OP^{DTT} of PM_{10} is roughly calculated based on the deposition efficiency of size-resolved PM by ICRP models and a hypothetical inhalation rate of 0.66 m^3 h^{-1}. The % are for mass concentrations.

Human health risks from the inhalation of elements were estimated based on their deposition fluxes. Our results indicated that in the whole respiratory tract, significant carcinogenic health risk was found for As, Co, and Cr (VI), mostly in $PM_{2.1-10}$ (>80%), with cancer risk values higher than the safety threshold 10^{-4} (Table 1), which shows that controlling $PM_{2.1-10}$ pollution is of great significance for human health protection. No significant carcinogenic or non-carcinogenic risks were found for other elements. The estimated results of As, Co, and Cr (VI) were similar to those for the outdoor PM-bound elements in Guangzhou, China, reported by Li et al. [53]. When considering specific position, PM-bound elements in the HA contributed the most (79.6–91.9%) to total health risks in the whole respiratory tract, with cancer risk values of As, Co, and Cr (VI) higher than the safety threshold 10^{-4}, followed by the PA (4.92–15.4%) and TB (3.21–5.36%) regions, with cancer risk values of As and Cr (VI) higher than the safety threshold 10^{-4} (Table S8). When considering PM size resolution, the health risks from $PM_{0.4}$-bound elements were the highest in the PA region and the lowest in the TB region, while $PM_{0.4-2.1}$- and $PM_{2.1-10}$-bound elements had the highest health risks in the HA and the lowest health risks in the TB region. Therefore, the contribution of elements in $PM_{0.4}$ and $PM_{0.4-2.1}$ to the total health risks increased with the increase in respiratory tract depth. For example, Cr (VI) in $PM_{0.4}$ accounted for 0.46% of health risks in the HA, which increased to 9.99% in the PA region. But in general, As, Co, and Cr (VI) in $PM_{2.1-10}$ contributed the most to cancer risk value compared with the elements in $PM_{0.4}$ and $PM_{0.4-2.1}$ in each part of the respiratory tract.

Table 1. Non-carcinogenic risks hazard quotient (HQ) and carcinogenic risks of selected elements in PM with different sizes by inhalation exposure.

Element	Non-Carcinogenic Risks (HQ)				Carcinogenic Risks			
	$PM_{0.4}$	$PM_{0.4-2.1}$	$PM_{2.1-10}$	SUM	$PM_{0.4}$	$PM_{0.4-2.1}$	$PM_{2.1-10}$	SUM
V	3.47×10^{-7}	6.34×10^{-6}	8.90×10^{-5}	9.56×10^{-5}	-	-	-	-
Cr	8.12×10^{-4}	7.71×10^{-3}	4.69×10^{-2}	5.54×10^{-2}	6.86×10^{-5}	6.51×10^{-4}	3.96×10^{-3}	**4.68×10^{-3}**
Mn	9.37×10^{-4}	$1.13 \times 101^{-}$	8.02×10^{-1}	9.16×10^{-1}	-	-	-	-
Fe	1.41×10^{-6}	4.93×10^{-5}	1.20×10^{-3}	1.25×10^{-3}	-	-	-	-
Co	1.55×10^{-4}	5.49×10^{-3}	4.63×10^{-2}	5.19×10^{-2}	6.10×10^{-7}	2.16×10^{-5}	1.82×10^{-4}	**2.04×10^{-4}**
Cu	1.80×10^{-7}	1.86×10^{-5}	1.65×10^{-4}	1.84×10^{-4}	-	-	-	-
Zn	2.16×10^{-6}	3.57×10^{-5}	1.57×10^{-4}	1.95×10^{-4}	-	-	-	-
As	1.64×10^{-5}	3.09×10^{-3}	1.50×10^{-2}	1.81×10^{-2}	5.25×10^{-6}	9.90×10^{-4}	4.80×10^{-3}	**5.79×10^{-3}**
Cd	3.92×10^{-7}	3.86×10^{-5}	5.15×10^{-5}	9.05×10^{-5}	1.73×10^{-7}	1.71×10^{-5}	2.28×10^{-5}	4.01×10^{-5}
Pb	3.11×10^{-6}	2.44×10^{-4}	1.19×10^{-3}	1.44×10^{-3}	2.15×10^{-7}	1.69×10^{-5}	8.25×10^{-5}	9.96×10^{-5}
Tl	8.04×10^{-7}	6.92×10^{-4}	7.67×10^{-4}	1.46×10^{-3}	-	-	-	-

Note: Bold means the risk is higher than the safety threshold 10^{-4}.

OP^{DTT}: As shown in the Section 2, OP^{DTT} is the DTT consumption rate of water-soluble oxidizing substances in PM. Here, we treated OP^{DTT} as a "pollutant" that could be deposited in the human respiratory tract. In the whole human respiratory tract, the average deposition flux of OP^{DTT} (defined as OP^{Flux}) of PM_{10} and its deposition efficiency were 1.19 ± 0.17 nmol min^{-1} h^{-1} and $64\% \pm 5.89\%$, respectively (Table S8 and Figure 2). The average OP^{Flux} (deposition efficiency) values were 0.98 ± 0.29 nmol min^{-1} h^{-1} ($53\% \pm 15.6\%$), 0.06 ± 0.01 nmol min^{-1} h^{-1} ($3\% \pm 0.91\%$), and 0.15 ± 0.05 nmol min^{-1} h^{-1} ($8\% \pm 2.18\%$) in the HA, TB, and PA regions of the respiratory tract, respectively. $PM_{2.1-10}$ contributed the most (73%) to total OP^{Flux} in the whole respiratory tract, and $PM_{0.4-2.1}$ and $PM_{0.4}$ accounted for 26% and 1%, respectively (Figure 2). The result that the predominant OP^{Flux} of PM_{10} was from $PM_{2.1-10}$ was consistent with the study by Guo et al. [54], but different from the reports from Fang et al. [33] and Lyu et al. [30] in which fine PM had the largest contribution to the total OP^{DTT} of PM in the whole pulmonary region.

When considering size resolution, the OP^{Flux} of $PM_{0.4}$ was the highest in the PA region (0.01 ± 0.001 nmol min^{-1} h^{-1}) and the lowest in the TB region (0.001 ± 0.001 nmol min^{-1} h^{-1}), while the OP^{Flux} of $PM_{0.4-2.1}$ and $PM_{2.1-10}$ was the highest in the HA and the lowest in the

TB region (Table S8). Levels of OP^{Flux} were bimodal with peaks at 3.3–4.7 and 5.8–9.0 μm in the HA, and were unimodal with peaks at 2.1–3.3 and 0.65–1.1 μm in the TB and PA regions, respectively (Figure S4). The contribution of PM$_{0.4}$ and PM$_{2.1–10}$ to total OP^{Flux} increased with the increase in respiratory tract depth. For example, the total contribution of them accounted for 22% of total OP^{Flux} in the HA, which increased to 64% in the PA region. Furthermore, the univariate linear regression analysis showed a significantly positive correlation between OP^{Flux} and the deposition of PM$_{2.1}$ mass; that is, with PM pollution aggravation in the air, for every 10-time increase in the deposition of PM$_{2.1}$, the OP^{Flux} increased by 0.12, 0.12, and 0.08 times in the HA, TB and PA regions, respectively (Figure S5). Similar, significantly positive correlations were also found between OP^{Flux} and the deposition of PM$_{2.1–10}$. Clinical studies reported that the abundance of natural antioxidants in the lung lining fluid decreases remarkably with an increase in respiratory tract depth [55], and antioxidants are believed to protect the respiratory system against the oxidative stress imposed by inhalable materials. In addition, smaller PM had a higher penetration in the PA regions of the respiratory tract [34]. Therefore, the oxidative impacts of PM$_{2.1}$ on the human respiratory system might require more attention than PM$_{2.1–10}$, especially when PM pollution is severe.

3.3. Association between OP$_v^{DTT}$ and PM-Bound Elements

To explore the association between OP$_v^{DTT}$ and the selected elements (V, Cr, Mn, Fe, Co, Cu, Zn, As, Cd, Pb, and Tl) in the PM in the air, Pearson correlation and univariate linear regression analyses were conducted (data points from all sites were pooled). Because the sampling time was during a season with stable meteorological conditions, and previous studies have shown that metals dominate OP [28,29], other potential confounding factors, such as other pollutants or environmental conditions, were neglected in our study.

For PM$_{0.4}$, OP$_v^{DTT}$ was strongly and positive correlated with concentrations of As ($r = 0.85$, $p < 0.01$) and Co ($r = 0.90$, $p < 0.01$) (Figure 3), and an IQR increase in their levels was associated with 53.8% (As, 95% CI: 28.9–78.5%) and 58.1% (Co, 95% CI: 17.6–98.6%) increases in OP$_v^{DTT}$ (Table 2). Previous studies have demonstrated that levels of As and Co in the air are highly affected by fossil fuel combustion (e.g., vehicle exhaust and coal burning) [45,46]. In addition, the high temperature of combustion is conducive to the formation of ROS, such as ·OH, ·O$_2-$, H$_2$O$_2$, and other free radicals [56,57], so it was not surprising to find a significantly positive correlation between OP$_v^{DTT}$ and elements associated with combustion sources.
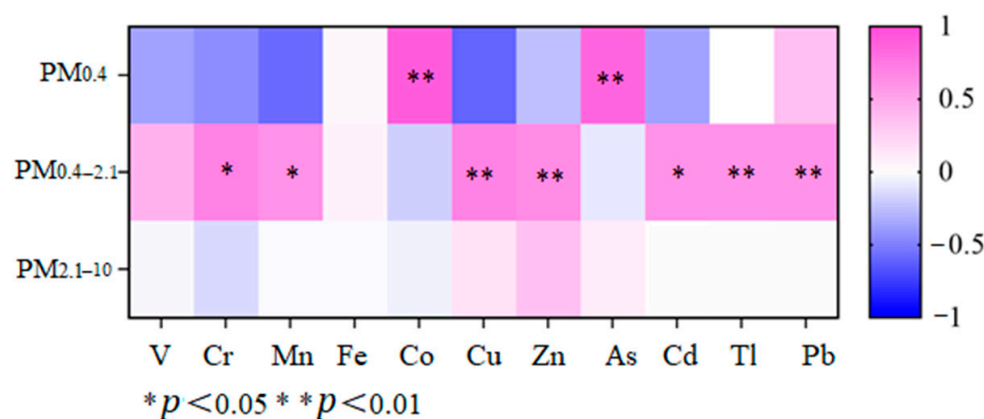
Figure 3. Heat map of Pearson coefficients between OP$_v^{DTT}$ (nmol min^{-1} m^{-3}) and concentrations of elements (ng m^{-3}) in air PM with different sizes.

Table 2. Association between OP_v^{DTT} (nmol min^{-1} m^{-3}) and concentrations (ng m^{-3}) of several selected elements in air PM (before respiratory exposure), and deposition flux association of OP^{DTT} (nmol min^{-1} h^{-1}) and elements (ng h^{-1}) in simplified human respiratory deposition model. (Linear regression analysis, confidence level = 95%.)

	Element	PM$_{0.4}$				PM$_{0.4-2.1}$			
		Slope β (95% CI)	Intercept α (95% CI)	R^2	IQR^{OP} (%) (95% CI)	Slope β (95% CI)	Intercept α (95% CI)	R^2	IQR^{OP} (%) (95% CI)
Before respiratory exposure [a]	V	-	-	-	-	-	-	-	-
	Cr	-	-	-	-	0.03 (0.00–0.06) **	−2.07 (−2.9–1.24)	0.60	52.2 (3.50–101)
	Mn	-	-	-	-	0.03 (0.02–0.05) **	−1.35 (−1.52--1.18)	0.73	21.6 (10.6–32.3)
	Fe	-	-	-	-	-	-	-	-
	Co	10.9 (6.91–15.0) **	−1.84 (−2.12--1.57)	0.91	58.1 (17.6–98.6)	-	-	-	-
	Cu	-	-	-	-	0.11 (0.06–0.17) **	−1.62 (−1.90--1.33)	0.61	27.5 (16.9–38.1)
	Zn	-	-	-	-	0.01 (0.01–0.02) **	−1.68 (−1.98--1.38)	0.61	31.6 (17.4–45.8)
	As	0.05 (0.02–0.07) **	−2.17 (−2.67--1.67)	0.85	53.8 (28.9–78.5)	-	-	-	-
	Cd	-	-	-	-	1.27 (0.51–2.01) **	−1.32 (−1.61--1.02)	0.73	20.8 (11.9–29.7)
	Tl	-	-	-	-	9.70 (6.04–13.4) **	−1.60 (−1.83--1.36)	0.60	26.7 (16.9–36.6)
	Pb	-	-	-	-	0.22 (0.12–0.33) **	−2.42 (−3.02--1.81)	0.67	26.7 (15.9–37.5)
After respiratory exposure [b]	V	-	-	-	-	0.62 (0.46–0.78) **	0.05 (0.03–0.06)	0.64	41.8 (18.0–65.6)
	Cr	-	-	-	-	0.01 (0.01–0.01) *	0.04 (0.00–0.09)	0.61	45.7 (−2.54–93.9)
	Mn	-	-	-	-	0.02 (0.01–0.02) **	0.04 (0.02–0.06)	0.63	42.9 (35.5–50.4)
	Fe [c]	-	-	-	-	0.08 (0.06–0.10) **	5.22 (3.29–7.15)	0.61	43.9 (−34.5–122)
	Co [d]	172 (108–235) **	−4.60 (−4.87--4.32)	0.91	58.1 (17.6–98.6)	-	-	-	-
	Cu	-	-	-	-	0.06 (0.04–0.07) **	0.05 (0.02–0.07)	0.67	42.8 (6.48–79.1)
	Zn [c]	-	-	-	-	0.35 (0.10–0.60) *	4.01 (3.08–11.1)	0.66	54.4 (4.91–104)
	As [d]	0.74 (0.38–1.11) **	−4.92 (−5.42--4.42)	0.85	53.8 (28.9–78.5)	-	-	-	-
	Cd	-	-	-	-	0.64 (0.50–0.78) **	0.05 (0.03–0.06)	0.73	41.7 (3.71–79.7)
	Tl	-	-	-	-	4.54 (3.64–5.44) **	0.04 (0.02–0.05)	0.75	45.0 (24.6–65.4)
	Pb	-	-	-	-	0.03 (0.02–0.04) **	0.04 (0.02–0.06)	0.74	44.8 (5.83–83.7)

[a]: The linear fitting is for concentrations of elements (independent variable) and OP_v^{DTT} (dependent variable), where OP_v^{DTT} was Ln-transformed. [b]: The linear fitting is for deposition flux of elements (independent variable) and OP^{DTT} (dependent variable). [c]: The deposition flux of OP^{DTT} was expanded 100 times. [d]: The deposition flux of OP^{DTT} was Ln-transformed. R^2: Fitting determination coefficient. ** *p*-valve < 0.01, * *p*-valve < 0.05. IQR^{OP}: Average percentage change in OP_v^{DTT} or deposition flux of OP^{DTT} per interquartile range (IQR) increase in concentrations or deposition flux of elements. -: No linear fitting relationship with R$^2 \geq 0.6$.

For PM$_{0.4-2.1}$, OP_v^{DTT} was positively correlated (moderately to strongly) with mass concentrations of Cr, Mn, Cu, Zn Cd, Tl, and Pb (*r* range: 0.60–0.84, *p* < 0.05) (Figure 3). The highest IQR increase in OP_v^{DTT} of 52.2% (95% CI: 3.50–101%) was associated with mass concentrations levels of Cr, and the IQR increase in OP_v^{DTT} for other elements was 21.6–31.6% (Table 2). The results indicated the selected elements might have a great impact on the OP_v^{DTT} of PM$_{0.4-2.1}$ in the plant, and similar results can be found in previous research [24,58]. For example, significantly positive correlations between OP_v^{DTT} and Cr, Co, Fe, Ni, Cu, Zn, Se, Mn, Cd, and Pb (*p* < 0.05) mass concentrations were observed in PM$_{2.5}$ collected from urban outdoor areas in the coastal cities by the Bohai Sea, northern China [59]. Significantly positive correlations between OP_v^{DTT} and V, Mn, Fe, Cu, As, Sr Ba, Li, Mg, Al, and Ti mass concentration were reported in PM$_{2.5}$ collected from urban outdoor areas in in Lahore and Peshawar, Pakistan [60]. However, negative or no correlation was also reported in studies conducted with air PM collected from the urban area of Milan, Northern Italy [26], and from central Atlanta, USA [27], where OP_v^{DTT} was mainly affected by water soluble-organic matter and brown carbon. Compared with PM$_{0.4}$, more elements were associated with the OP_v^{DTT} in PM$_{0.4-2.1}$ in our study. This might be related to the higher fractions of nitrate and sulfate in PM$_{0.4-2.1}$, which can dissolve more metals. Moreover, the long residence time and the long-distance transport capacity of PM$_{0.4-2.1}$ in the air can also lead to more ROS or free radical generation through metal catalysis during PM aging [30,31,33].

For $PM_{2.1-10}$, no significant correlation was found between OP_v^{DTT} and elements' mass concentrations. However, significantly positive correlations between OP_v^{DTT} and V, Fe, and Cu mass concentrations were reported in $PM_{2.5-10}$ collected from an animal farm, a continuous traffic site, a Stop&Go traffic site, and an urban background site in the Netherlands [25].

Generally speaking, on their surface, particles contain soluble transition metals such as Fe, Cu, Mn, Cr, and V that can generate ROS through Fenton-type reactions and act as catalysts by Haber–Weiss reactions (Figure 4) [7,28]. Taking Fe as an example, ferrous iron (Fe^{2+}) reduces hydrogen peroxide (H_2O_2) with the formation of hydroxyl radicals (•OH) and the oxidation of ferrous iron to ferric iron (Fe^{3+}). This reaction can be recycled by reductants such as superoxide anions, DTT glutathione, and ascorbic acid by reducing Fe^{3+} to Fe^{2+}. All ROS were measured from the oxidation of DTT. Because only the soluble forms of metals participate in redox reactions, correlations between OP_v^{DTT} and total metal mass concentrations depend on the fraction of total metal that is soluble. Moreover, the different correlations between OP and elements in PM with different sizes are influenced by chemical form, oxidation and reduction behavior, and capacity of ROS generation or induction, for example, Fenton-type, Haber–Weiss reactions, etc. [12,28]. Moreover, correlations do not show causal relationships between OP assays and PM components, especially since particulate species are often highly covariate [28]. More research on the solubility and morphology of metals is needed to reveal their correlation mechanisms.
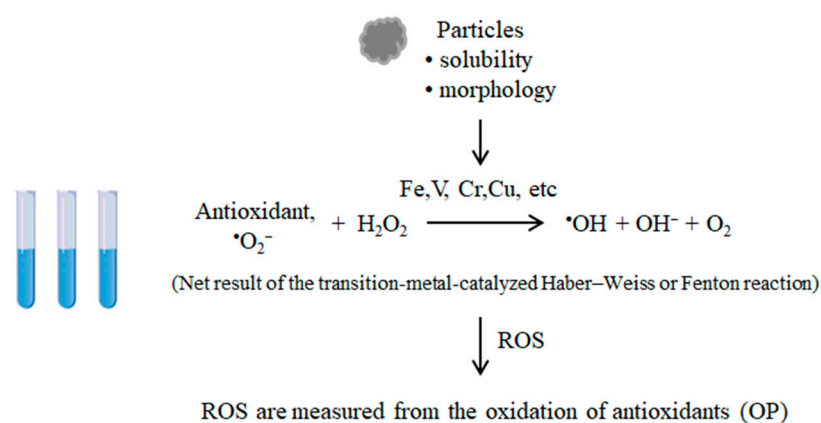

Figure 4. Graphical mechanism of significant and positive correlations between mass concentrations of transition metals and OP.

3.4. Association between OP^{Flux} and Elements after Respiratory Exposure

As OP may be a better reference value to explain the biological effects of PM exposure than PM concentration [16,17], the relationship between OP^{Flux} and the deposition flux of elements in the human respiratory tract may give more specific information to understand the potential risks of PM exposure. We tested the relationship between OP^{Flux} and the deposition flux of selected elements (V, Cr, Mn, Fe, Co, Cu, Zn, As, Cd, Pb, and Tl) calculated based on the simplified human respiratory deposition model using Pearson correlation and univariate linear regression models (data points from all sites were pooled).

When considering PM size, strong and positive correlations were found between the deposition flux of As or Co and OP^{Flux} in $PM_{0.4}$ ($r > 0.85$, Figure 5), similar to those in OP_v^{DTT} and PM-bound elements in the air, because in the respiratory tract model, $PM_{0.4}$ only had one size classification and deposited in the respiratory tract with a fixed deposition efficiency. It is worth noting that in $PM_{0.4-2.1}$, the correlation coefficients between element deposition flux and OP^{Flux} (r: 0.69–0.86) were higher than the values between OP_v^{DTT} and element concentrations. For example, the IQR increases in deposition flux of V, Cr, Mn, Fe, Cu, Zn, Cd, Tl, and Pb (ng h^{-1}) were associated with a 41.7–54.4% increase in OP^{Flux} (Table 2). The elevated relation between OP^{Flux} and the deposition flux of elements compared with those between OP_v^{DTT} and PM-bound elements in air $PM_{0.4-2.1}$ may indicate

the contrition of elements to OP of PM was intensified after inhalation. Therefore, the association between OP^{Flux} and the deposition flux of elements in the respiratory tract may provide a useful reference to understand the relationship between element external exposure and potential human health effects.
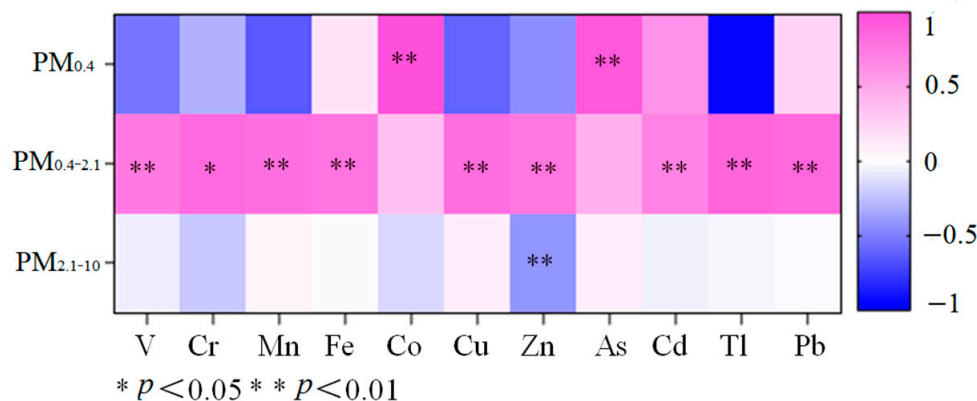
Figure 5. Heat map of Pearson coefficients between deposition fluxes of OP^{DTT} (nmol min^{-1} h^{-1}) and elements (ng h^{-1}) in PM with different sizes in the whole respiratory tract.

4. Conclusions

This study reported on size-resolved elements and OP in air PM collected from a waste recycling plant. Compared with $PM_{0.4}$ and $PM_{0.4-2.1}$, $PM_{2.1-10}$ contributed the most to total OP^{DTT} and its bound elements contributed the most to potential health risks. After the inhalation model simulation, $PM_{2.1-10}$ contributed the highest (73%) to total OP^{Flux} in the whole respiratory tract, followed by $PM_{0.4-2.1}$ (26%) and $PM_{0.4}$ (1%). The association between OP_v^{DTT} and elements' mass concentrations varied with PM size, and was not found in $PM_{2.1-10}$. However, significant and positive correlations were found between several elements' mass concentrations and OP_v^{DTT} in $PM_{0.4}$ and $PM_{0.4-2.1}$ (r: 0.60–0.90). So, other chemicals other than the targeted elements may contribute to $PM_{2.1-10}$ in the air. After the respiratory exposure model simulation, the relationship between OP^{Flux} and the deposition flux of the targeted elements was intensified compared with those between OP_v^{DTT} and PM-bound elements' mass concentrations in air PM_{10}.

This study focuses on a specific waste recycling plant, which enriches the knowledge of the association between OP^{DTT} and the chemical composition in PM of different sizes, especially after respiratory exposure. However, our study also has several limitations. For example, this study is a special case, which may limit the generalizability of the findings to other settings or regions. It would be valuable to study a more diverse range of sampling locations to enhance the external validity of the study. In addition, the number of samples was not large enough. Increasing the sample size and duration of data collection could obtain more robust and representative results.

parameters for health risk assessment of elements via inhalation pathway [61,62]; Table S3. Oral reference dose (RfD) (mg kg^{-1} day^{-1}) and cancer slope factor (CSF) (kg·day mg^{-1}) of elements; Table S4. Values (mean ± standard deviation) of element concentratons (ng m^{-3}), and OPmDTT (pmol min^{-1} μg^{-1}) and OPvDTT (nmol min^{-1}m^{-3}) of PM with different sizes in the waste recycle plant, South China; Table S5. Relationships between enrichment factor (EF) and enrichment degree of the studied elements; Table S6. Enrichment factor of elements in PM with different sizes in the waste recycle plant, South China; Table S7. Comparison of OPmDTT (pmol min^{-1} μg^{-1}) and OPvDTT (nmol min^{-1}m^{-3}) in PM with different sizes around the world [63–70]; Table S8: Deposition fluxes of OPDTT (nmol min^{-1} h^{-1}) and elements (ng h^{-1}) in PM with different sizes in the whole respiratory tract and health risks of elements in different positions of respiratory tract.

Author Contributions: X.L.: Data curation, original draft preparation and editing. T.X.: Sampling; Y.G.: Conceptualization, supervision, and editing. All authors have read and agreed to the published version of the manuscript.

Institutional Review Board Statement: Not applicable.

Informed Consent Statement: Not applicable.

Data Availability Statement: Data is contained within the article or Supplementary Materials.

Conflicts of Interest: The authors declare no competing interests.

References

1. Zhang, S.Y.; Qian, Z.M.; Chen, L.; Zhao, X.; Cai, M.; Wang, C.J.; Zou, H.T.; Wu, Y.L.; Zhang, Z.L.; Li, H.T.; et al. Exposure to Air Pollution during Pre-Hypertension and Subsequent Hypertension, Cardiovascular Disease, and Death: A Trajectory Analysis of the UK Biobank Cohort. *Environ. Health Perspect.* **2023**, *131*, 17008. [CrossRef]
2. Wang, R.Z.; Liu, J.J.; Qin, Y.H.; Chen, Z.; Li, J.C.; Guo, P.F.; Shan, L.H.; Li, Y.; Hao, Y.H.; Jiao, M.L.; et al. Global attributed burden of death for air pollution: Demographic decomposition and birth cohort effect. *Sci. Total Environ.* **2023**, *860*, 160444. [CrossRef]
3. Leitte, A.M.; Schlink, U.; Herbarth, O.; Wiedensohler, A.; Pan, X.C.; Hu, M.; Richter, M.; Wehner, B.; Tuch, T.; Wu, Z.J.; et al. Size-segregated particle number concentrations and respiratory emergency room visits in Beijing, China. *Environ. Health Perspect.* **2011**, *119*, 508–513. [CrossRef]
4. Weichenthal, S.; Lavigne, E.; Traub, A.; Umbrio, D.; You, H.Y.; Pollitt, K.; Shin, T.; Kulka, R.; Stieb, D.M.; Korsiak, J.; et al. Association of sulfur, transition metals, and the oxidative potential of outdoor PM$_{2.5}$ with acute cardiovascular events: A case-crossover study of Canadian adults. *Environ. Health Perspect.* **2021**, *129*, 107005. [CrossRef]
5. Hu, J.; Zhou, R.X.; Ding, R.; Ye, D.W.; Su, Y.B. Effect of PM$_{2.5}$ air pollution on the global burden of lower respiratory infections, 1990–2019: A systematic analysis from the Global Burden of Disease Study 2019. *J. Hazard. Mater.* **2023**, *459*, 132215. [CrossRef]
6. Sang, S.W.; Zhang, T.C.; Zhang, Y.; Chen, H.; Sang, S.W. The global burden of disease attributable to ambient fine particulate matter in 204 countries and territories, 1990–2019: A systematic analysis of the Global Burden of Disease Study 2019. *Ecotoxicol. Environ. Saf.* **2022**, *238*, 113588. [CrossRef]
7. Risom, L.; Moller, P.; Loft, S. Oxidative stress-induced DNA damage by particulate air pollution. *Mutat. Res.* **2005**, *592*, 119–137. [CrossRef]
8. Tao, F.; Gonzalez-Flecha, B.; Kobzik, L. Reactive oxygen species in pulmonary inflammation by ambient particulates. *Free Radic. Biol. Med.* **2003**, *35*, 327–340. [CrossRef]
9. Saffari, A.; Daher, N.; Shafer, M.M.; Schauer, J.J.; Sioutas, C. Global perspective on the oxidative potential of airborne particulate matter: A synthesis of research findings. *Environ. Sci. Technol.* **2014**, *48*, 7576–7583. [CrossRef]
10. Yang, J.C.; Roth, P.; Ruehl, C.R.; Shafer, M.M.; Antkiewicz, D.S.; Durbin, T.D.; Cocker, D.; Asa-Awukua, A.; Karavalakis, G. Physical, chemical, and toxicological characteristics of particulate emissions from current technology gasoline direct injection vehicles. *Sci. Total Environ.* **2019**, *650*, 1182–1194. [CrossRef]
11. Bates, J.T.; Fang, T.; Verma, V.; Zeng, L.H.; Weber, R.J.; Tolbert, P.E.; Abrams, J.Y.; Sarnat, S.E.; Klein, M.; Mulholland, J.A.; et al. Review of acellular assays of ambient particulate matter oxidative potential: Methods and relationships with composition, sources, and health effects. *Environ. Sci. Technol.* **2019**, *53*, 4003–4019. [CrossRef]
12. Szigeti, T.; Kertész, Z.; Dunster, C.; Kelly, F.J.; Záray, G.; Mihucz, V.G. Exposure to PM$_{2.5}$ in modern office buildings through elemental characterization and oxidative potential. *Atmos. Environ.* **2014**, *94*, 44–52. [CrossRef]
13. Verma, V.; Fang, T.; Xu, L.; Peltier, R.E.; Russell, A.G.; Ng, N.L.; Weber, R.J. Organic aerosols associated with the generation of reactive oxygen species (ROS) by water-soluble PM$_{2.5}$. *Environ. Sci. Technol.* **2015**, *49*, 4646–4656. [CrossRef]

14. Exposito, A.; Markiv, B.; Santibáñez, M.; Fadel, M.; Ledoux, F.; Courcot, D.; Fernández-Olmo, I. Ascorbate oxidation driven by $PM_{2.5}$-bound metal(loid)s extracted in an acidic simulated lung fluid in relation to their bioaccessibility. *Air Qual. Atmos. Health* **2024**, *17*, 177–189. [CrossRef]

15. Pietrogrande, M.C.; Bertoli, I.; Manarini, F.; Russo, M. Ascorbate assay as a measure of oxidative potential for ambient particles: Evidence for the importance of cell-free surrogate lung fluid composition. *Atmos. Environ.* **2019**, *211*, 103–112. [CrossRef]

16. Abrams, J.Y.; Weber, R.J.; Klein, M.; Sarnat, S.E.; Chang, H.H.; Strickland, M.J.; Verma, V.; Fang, T.; Bates, J.T.; Mulholland, J.A.; et al. Associations between ambient fine particulate oxidative potential and cardiorespiratory emergency department visits. *Environ. Health Perspect* **2017**, *125*, 107008. [CrossRef]

17. Bates, J.T.; Weber, R.J.; Abrams, J.; Verma, V.; Fang, T.; Klein, M.; Strickland, M.J.; Sarnat, S.E.; Chang, H.H.; Mulholland, J.A.; et al. Reactive oxygen species generation linked to sources of atmospheric particulate matter and cardiorespiratory effects. *Environ. Sci. Technol.* **2016**, *49*, 13605–13612. [CrossRef]

18. Schiavo, B.; Meza-Figueroa, D.; Vizuete-Jaramillo, E.; Robles-Morua, A.; Angulo-Molina, A.; Reyes-Castro, P.A.; Inguaggiato, C.; Gonzalez-Grijalva, B.; Pedroza-Montero, M. Oxidative potential of metal-polluted urban dust as a potential environmental stressor for chronic diseases. *Environ. Geochem. Health* **2023**, *45*, 3229–3250. [CrossRef]

19. Daellenbach, K.R.; Uzu, G.; Jiang, J.H.; Cassagnes, L.E.; Leni, Z.; Vlachou, A.; Stefenelli, G.; Canonaco, F.; Weber, S.; Segers, A.; et al. Sources of particulate-matter air pollution and its oxidative potential in Europe. *Nature* **2020**, *587*, 414–419. [CrossRef]

20. Hu, S.; Polidori, A.; Arhami, M.; Shafer, M.M.; Schauer, J.J.; Cho, A.; Sioutas, C. Redox activity and chemical speciation of size fractioned PM in the communities of the Los Angeles-Long Beach Harbor. *Atmos. Chem. Phys.* **2008**, *8*, 6439–6451. [CrossRef]

21. Khaled, A.; Zhang, M.; Ervens, B. The number fraction of iron-containing particles affects OH, HO_2 and H_2O_2 budgets in the atmospheric aqueous phase. *Atmos. Chem. Phys.* **2021**, *3*, 1989–2009.

22. Qin, L.J.; Yang, L.L.; Yang, J.H.; Weber, R.; Ranguelova, K.; Liu, X.Y.; Lin, B.C.; Li, C.; Zheng, M.H.; Liu, G.R. Photoinduced formation of persistent free radicals, hydrogen radicals and hydroxyl radicals from catechol on atmospheric particulate matter. *iScience* **2021**, *24*, 102193. [CrossRef] [PubMed]

23. Deguillaume, L.; Leriche, M.; Desboeufs, K.; Mailhot, G.; George, C.; Chaumerliac, N. Transition metals in atmospheric liquid phases: Sources, reactivity, and sensitive parameters. *Chem. Rev.* **2005**, *105*, 3388–3431. [CrossRef] [PubMed]

24. Verma, V.; Shafer, M.M.; Schauer, J.J.; Sioutas, C. Contribution of transition metals in the reactive oxygen species activity of PM emissions from retrofitted heavy-duty vehicles. *Atmos. Environ.* **2010**, *44*, 5165–5173. [CrossRef]

25. Janssen, N.A.H.; Yang, A.L.; Strak, M.; Steenhof, M.; Hellack, B.; Gerlofs-Nijland, M.E.; Kuhlbusch, T.; Kelly, F.; Harrison, R.M.; Brunekreef, B.; et al. Oxidative potential of particulate matter collected at sites with different source characteristics. *Sci. Total Environ.* **2014**, *472*, 572–581. [CrossRef] [PubMed]

26. Perrone, M.G.; Zhou, J.; Malandrino, M.; Sangiorgi, G.; Rizzi, C.; Ferrero, L.; Dommen, J.; Bolzacchini, E. PM chemical composition and oxidative potential of the soluble fraction of particles at two sites in the urban area of Milan, northern Italy. *Atmos. Environ.* **2016**, *128*, 104–113. [CrossRef]

27. Verma, V.; Rico-Martinez, R.; Kotra, N.; King, L.; Liu, J.M.; Snell, T.W.; Weber, R.J. Contribution of water-soluble and insoluble components and their hydrophobic/hydrophilic subfractions to the reactive oxygen species-generating potential of fine ambient aerosols. *Environ. Sci. Technol.* **2012**, *46*, 11384–11392. [CrossRef] [PubMed]

28. Charrier, J.G.; Anastasio, C. On dithiothreitol (DTT) as a measure of oxidative potential for ambient particles: Evidence for the importance of soluble transition metals. *Atmos. Chem. Phys.* **2012**, *12*, 9321–9333. [CrossRef]

29. Charrier, J.G.; Richards-Henderson, N.K.; Bein, K.J.; McFall, A.S.; Wexler, A.S.; Anastasio, C. Oxidant production from source-oriented particulate matter—Part 1: Oxidative potential using the dithiothreitol (DTT) assay. *Atmos. Chem. Phys.* **2015**, *15*, 2327–2340. [CrossRef]

30. Lyu, Y.; Guo, H.B.; Cheng, T.T.; Li, X. Particle size distributions of oxidative potential of lung-deposited particles: Assessing contributions from quinones and water-soluble metals. *Environ. Sci. Technol.* **2018**, *52*, 6592–6600. [CrossRef]

31. Fang, T.; Guo, H.Y.; Zeng, L.H.; Verma, V.; Nenes, A.; Weber, R.J. Highly acidic ambient particles, soluble metals, and oxidative potential: A Link between sulfate and aerosol toxicity. *Environ. Sci. Technol.* **2017**, *51*, 2611–2620. [CrossRef]

32. Zhang, X.; Staimer, N.; Tjoa, T.; Gillen, D.L.; Schauer, J.J.; Shafer, M.M.; Hasheminassab, S.; Pakbin, P.; Longhurst, J.; Sioutas, C.; et al. Associations between microvascular function and short-term exposure to traffic-related air pollution and particulate matter oxidative potential. *Environ. Health* **2016**, *15*, 81. [CrossRef]

33. Fang, T.; Zeng, L.H.; Gao, D.; Verma, V.; Stefaniak, A.B.; Weber, R.J. Ambient size distributions and lung deposition of aerosol dithiothreitol-measured oxidative potential: Contrast between soluble and insoluble particles. *Environ. Sci. Technol.* **2017**, *51*, 6802–6811. [CrossRef] [PubMed]

34. Yeh, H.C.; Cuddihy, R.G.; Phalen, R.F.; Chang, I.Y. Comparisons of Calculated Respiratory Tract Deposition of Particles Based on the Proposed NCRP Model and the New ICRP66 Model. *Aerosol Sci. Technol.* **1996**, *25*, 134–140. [CrossRef]

35. Liu, Z.; Gao, W.K.; Yu, Y.C.; Hu, B.; Xin, J.Y.; Sun, Y.; Wang, L.L.; Wang, G.H.; Bi, X.H.; Zhang, G.H.; et al. Characteristics of $PM_{2.5}$ mass concentrations and chemical species in urban and background areas of China: Emerging results from the CARE-China network. *Atmos. Chem. Phys.* **2018**, *18*, 8849–8871. [CrossRef]

36. Wang, Y.H.; Tang, G.Q.; Zhao, W.; Yang, Y.; Wang, L.L.; Liu, Z.R.; Wen, T.X.; Cheng, M.T.; Wang, Y.M.; Wang, Y.S. Different roles of nitrate and sulfate in air pollution episodes in the North China Plain. *Atmos. Environ.* **2020**, *224*, 117325. [CrossRef]

37. Bailey, M.R. The new ICRP model for the respiratory tract. *Radiat. Prot. Dosim.* **1994**, *53*, 107–114. [CrossRef]

38. Bailey, M.R.; Ansoborlo, E.; Guilmette, R.A.; Paquet, F. Updating the ICRP human respiratory tract model. *Radiat. Prot. Dosim.* **2007**, *127*, 31–34. [CrossRef]

39. USEPA. *Exposure Factors Handbook*, 2011th ed.; National Center for Environmental Assessment: Washington, DC, USA, 2011.

40. USEPA. *Risk Assessment Guidance for Superfund. Volume I: Human Health Evaluation Manual (Part A)*; United States Environmental Protection Agency: Washington, DC, USA, 1989.

41. Tan, J.; Duan, J. Heavy metals in aerosol in China: Pollution, sources, and control strategies. *J. Grad. Univ. Chin. Acad. Sci.* **2013**, *30*, 145–155.

42. USEPA. *Risk Assessment Guidance for Superfund. Part A: Human Health Evaluation Manual; Part E, Supplemental Guidance for Dermal Risk Assessment; Part F, Supplemental Guidance for Inhalation Risk Assessment*; United States Environmental Protection Agency: Washington, DC, USA, 2011.

43. Zhang, J.; Zhou, X.H.J.; Wang, Z.; Yang, L.X.; Wang, J.; Wang, W.X. Trace elements in $PM_{2.5}$ in Shandong province: Source identification and health risk assessment. *Sci. Total Environ.* **2018**, *621*, 558–577. [CrossRef]

44. Li, M.; Gao, Y.H.; Guo, L.C.; Lian, X.W.; Yao, J. Primary research on health risk assessment of heavy metals in air $PM_{2.5}$ in Guangzhou. *J. Environ. Health* **2016**, *33*, 421–424.

45. Zhi, M.; Zhang, X.; Zhang, K.; Ussher, S.J.; Lv, W.L.; Li, J.; Gao, J.; Luo, Y.Q.; Meng, F. The characteristics of atmospheric particles and metal elements during winter in Beijing: Size distribution, source analysis, and environmental risk assessment. *Ecotoxicol. Environ. Saf.* **2021**, *211*, 111937. [CrossRef]

46. Tian, Y.Z.; Li, Y.X.; Liang, Y.L.; Xue, Q.Q.; Feng, X.; Feng, Y.C. Size distributions of source-specific risks of atmospheric heavy metals: An advanced method to quantify source contributions to size-segregated respiratory exposure. *J. Hazard. Mater.* **2020**, *407*, 124355. [CrossRef]

47. Boreddy, S.K.R.; Hegde, P.; Aswini, A.R. Geochemical characteristics of trace elements in size-resolved coastal urban aerosols associated with distinct air masses over tropical peninsular India: Size distributions and source apportionment. *Sci. Total Environ.* **2020**, *763*, 142967. [CrossRef]

48. Yu, H.; Zhao, X.Y.; Wang, J.; Yin, B.H.; Geng, C.M.; Wang, X.H.; Gu, C.; Huang, L.H.; Yang, W.; Bai, Z.P. Chemical characteristics of road dust $PM_{2.5}$ fraction in oasis cities at the margin of Tarim Basin. *J. Environ. Sci.* **2020**, *95*, 217–224. [CrossRef]

49. Liu, B.S.; Song, N.; Dai, Q.L.; Mei, R.B.; Sui, B.H.; Bi, X.H.; Feng, Y.C. Chemical composition and source apportionment of ambient $PM_{2.5}$ during the non-heating period in Taian, China. *Atmos. Res.* **2016**, *170*, 23–33. [CrossRef]

50. Wei, F.S.; Chen, J.S.; Wu, Y.Y.; Zheng, C.J. *Introduction to Background Value of Soil Environment*; China Environmental Science Press: Beijing, China; China Ministry of Environmental Protection: Beijing, China, 1990.

51. Daher, N.; Saliba, N.A.; Shihadeh, A.L.; Jaafar, M.; Baalbaki, R.; Shafer, M.M.; Schauer, J.J.; Sioutas, C. Oxidative potential and chemical speciation of size-resolved particulate matter (PM) at near-freeway and urban background sites in the greater Beirut area. *Sci. Total Environ.* **2014**, *470*, 417–426. [CrossRef]

52. Wu, N.; Lu, B.Q.; Chen, J.M.; Li, X. Size distributions of particle-generated hydroxyl radical (·OH) in surrogate lung fluid (SLF) solution and their potential sources. *Environ. Pollut.* **2020**, *268*, 115582. [CrossRef]

53. Li, F.; Yan, J.J.; Wei, Y.C.; Zeng, J.J.; Wang, X.Y.; Chen, X.Y.; Zhang, C.R.; Li, W.D.; Chen, M.; Lü, G.N. $PM_{2.5}$-bound heavy metals from the major cities in China: Spatiotemporal distribution, fuzzy exposure assessment and health risk management. *J. Clean. Prod.* **2020**, *286*, 124967. [CrossRef]

54. Guo, H.B.; Li, M.; Lyu, Y.; Cheng, T.T.; Xv, J.J.; Li, X. Size-resolved particle oxidative potential in the office, laboratory, and home: Evidence for the importance of water-soluble transition metals. *Environ. Pollut.* **2019**, *246*, 704–709. [CrossRef]

55. Kelly, F.J. Oxidative stress: Its role in air pollution and adverse health effects. *Occup. Environ. Med.* **2003**, *60*, 612–616. [CrossRef] [PubMed]

56. Saffari, A.; Daher, N.; Shafer, M.M.; Schauer, J.J.; Sioutas, C. Seasonal and spatial variation in dithiothreitol (DTT) activity of quasi-ultrafine particles in the Los Angeles Basin and its association with chemical species. *Environ. Lett.* **2014**, *49*, 441–451. [CrossRef] [PubMed]

57. Gehling, W.; Dellinger, B. Environmentally persistent free radicals and their lifetimes in $PM_{2.5}$. *Environ. Sci. Technol.* **2013**, *47*, 8172–8178. [CrossRef]

58. Yu, S.Y.; Liu, W.J.; Xu, Y.S.; Yi, K.; Zhou, M.; Tao, S.; Liu, W.X. Characteristics and oxidative potential of atmospheric $PM_{2.5}$ in Beijing: Source apportionment and seasonal variation. *Sci. Total Environ.* **2019**, *650*, 277–287. [CrossRef]

59. Liu, W.; Xu, Y.S.; Liu, W.X.; Liu, Q.Y.; Yu, S.Y.; Liu, Y.; Wang, X.; Tao, S. Oxidative potential of ambient $PM_{2.5}$ in the coastal cities of the Bohai Sea, northern China: Seasonal variation and source apportionment. *Environ. Pollut.* **2018**, *236*, 514–528. [CrossRef]

60. Ahmad, M.; Yu, Q.; Chen, J.; Cheng, S.M.; Qin, W.H.; Zhang, Y.P. Chemical characteristics, oxidative potential, and sources of $PM_{2.5}$ in wintertime in Lahore and Peshawar, Pakistan. *J. Environ. Sci.* **2021**, *102*, 11.

61. USEPA. *Risk Assessment Guidance for Superfund: Volume III—Part A, Process for Conducting Probabilistic Risk Assessment*; United States Environmental Protection Agency: Washington, DC, USA, 2001. Available online: https://semspub.epa.gov/work/HQ/134487.pdf (accessed on 29 February 2024).

62. USEPA. *Risk Assessment Guidance for Superfund: Volume I—Human Health Evaluation Manual—Part E, Supplemental Guidance for Dermal Risk Assessment*; United States Environmental Protection Agency: Washington, DC, USA, 2004. Available online: https://www.epa.gov/risk/risk-assessment-guidance-superfund-rags-part-e (accessed on 29 February 2024).

63. Verma, V.; Fang, T.; Guo, H.; King, L.; Bates, J.T.; Peltier, R.E.; Edgerton, E.; Russell, A.G.; Weber, R.J. Reactive oxygen species associated with water-soluble $PM_{2.5}$ in the southeastern United States: Spatiotemporal trends and source apportionment. *Atmos. Chem. Phys.* **2014**, *14*, 19625–19672. [CrossRef]

64. Vreeland, H.; Schauer, J.J.; Russell, A.G.; Marshall, J.D.; Fushimi, A.; Jain, G.; Sethuraman, K.; Verma, V.; Tripathi, S.N.; Bergin, M.H. Chemical characterization and toxicity of particulate matter emissions from roadside trash combustion in urban India. *Atmos. Environ.* **2016**, *147*, 22–30. [CrossRef]

65. Romano, S.; Becagli, S.; Lucarelli, F.; Russo, M.; Pietrogrande, M.C. Oxidative Potential Sensitivity to Metals, Br, P, S, and Se in PM_{10} Samples: New Insights from a Monitoring Campaign in Southeastern Italy. *Atmosphere* **2020**, *11*, 367. [CrossRef]

66. Sauvain, J.J.; Deslarzes, S.; Storti, F.; Riediker, M. Oxidative Potential of Particles in Different Occupational Environments: A Pilot Study. *Ann. Occup. Hyg.* **2015**, *59*, 882–894. [CrossRef]

67. Brehmer, C.; Lai, A.M.; Clark, S.; Shan, M.; Carter, E.M. The Oxidative Potential of Personal and Household PM2.5 in a Rural Setting in Southwestern China. *Environ. Sci. Technol.* **2019**, *53*, 2788–2798. [CrossRef] [PubMed]

68. Wang, Y.; Wang, M.; Li, S..; Sun, H.; Mu, Z.; Zhang, L.; Li, Y.; Chen, Q. Study on the oxidation potential of the water-soluble components of ambient $PM_{2.5}$ over Xi'an, China: Pollution levels, source apportionment and transport pathways. *Environ. Int.* **2020**, *136*, 105515. [CrossRef]

69. Zhang, Y.J.; Cong, H.; Lv, Y.S.; Ma, S.X.; Ying, G.; Zeng, E.Y. Polycyclic aromatic hydrocarbon exposure, oxidative potential in dust, and their relationships to oxidative stress in human body: A case study in the indoor environment of Guangzhou, South China. *Environ. Int.* **2021**, *149*, 106405. [CrossRef] [PubMed]

70. Jin, W.; Su, S.; Wang, B.; Zhu, X.; Chen, Y.; Shen, G.; Liu, J.; Cheng, H.; Wang, X.; Wu, S. Properties and cellular effects of particulate matter from direct emissions and ambient sources. *J. Environ. Sci. Health Part A Toxic Hazard. Subst. Environ. Eng.* **2016**, *51*, 1075–1083. [CrossRef] [PubMed]